LA-UR- 03-1103.

Approved for public release; distribution is unlimited.

Title:	Transverse Texture and Microstructure Gradients in Friction-Stir Welded 2519 Aluminum
Author(s):	John F. Bingert, ADWP, LANL Richard W. Fonda, Naval Research Laboratory, Wash., DC
Submitted to:	Proceedings of the 4th International Symposium on Friction Stir Welding Park City, UT May 14-16, 2003

Transverse Texture and Microstructure Gradients in Friction-Stir Welded 2519 Aluminum

J.F. Bingert[1] and R.W. Fonda[2]
[1]*Los Alamos National Laboratory, Los Alamos, NM**
[2]*Naval Research Laboratory, Washington, DC*
**on change-of-station to Naval Research Laboratory*

Abstract

Friction-stir welding produces severe thermomechanical transients that generate crystallographic texture evolution throughout the weld-affected microstructure. In this study, a friction stir weld in a coarse-grained 2519 aluminum plate was investigated in order to resolve the influence of these thermal and deformation effects on texture and microstructure development. Automated electron backscatter diffraction (EBSD) was applied to spatially resolve orientations in the base metal, weld nugget, and thermomechanical and heat-affected zones. Results show a gradient demarcated by an alteration in boundary character, texture, and precipitate distribution between the thermomechanical affected zone and the recrystallized weld nugget. EBSD scans and microstructural characterizations reveal substructure evolution from the base plate to the nugget indicative of dynamic recovery and recrystallization processes. Experimental results of texture evolution, however, did not directly follow from considerations of simplified deformation gradients and resultant simple-shear textures resulting from restricted glide.

1. Introduction

The growth of friction-stir welding (FSW) as a viable commercial joining technique has progressed more rapidly than the understanding of process-structure-property relationships for this complex processing system. Among significant microstructural parameters that may affect mechanical and environmental response of the weld is the distribution of boundary structure and crystallographic orientations, or texture, especially as a function of relative position in the weld.

Previous studies of the microstructural zones in friction stir welds have led to a general consensus on the development of certain features [1-3]. Moving from the base plate to the center of the weld, microstructurally discrete regions are comprised of a heat affected zone (HAZ), thermomechanical affected zone (TMAZ), and the recrystallized weld nugget. The microstructures are distinguished by precipitation, shear deformation, substructure development, and dynamic recrystallization. The dominant stress state produced by the rotating pin and shoulder is simple shear. However, the shear plane and direction are dependent on position in the weld; nearer the surface the shoulder shear dominates with a shear plane parallel to the top surface, while nearer the pin the plane with the largest shear is aligned in the through-thickness direction. Gradients between the two extremes may be expected in other locations. Superimposed on the shears is the flow of material downward due to the mechanical action of the threaded pin tool. This macroscopic flow results in a counterflow extrusion from the base plate toward the top of the weld to replace the vacated material. More complex pin geometries incorporate threads in both directions to facilitate this material flow. Thermomechanical excursions are sufficient to dynamically recrystallize aluminum only in the center nugget region, and it must be emphasized that the FSW process

is solid state. The combination of shear, extrusion, frictional heat, and recrystallization results in the typical cross-sectional microstructure consisting of an "onion ring" comprised of the recrystallized nugget, surrounded by a pattern of elongated grains indicating the flow of material from the base plate in response to the pin movement.

Previous studies on the texture development in FSWs by Sato, *et al.* on 6063 Al [3] and Field, *et al.* on 1100 and 6061 Al [4] described the effect of the simple shear deformation state on texture evolution. Jin, *et al.* [1] have observed weakening of the deformation texture in the recrystallized weld nugget, with less direct correspondence of the texture to the shear deformation. In this study, the friction stir zone from a 2519 aluminum plate weldment was investigated in order to determine the evolution of texture and boundary structure from the base plate to the weld nugget along the transverse direction, especially at the interface between the TMAZ and nugget where recrystallization effects are introduced. Automated electron backscatter diffraction (EBSD) [5] was used in conjunction with standard metallography to interrogate the microstructural evolution of material as it was affected by the thermal and deformation gradients. The texture may function as a forensic means to ascertain the thermomechanical history. The objective of this study was to characterize the HAZ, TMAZ, and nugget regions, and especially the microstructural gradients near their transitions in detail to gain insight into the microstructure-altering conditions present during welding. In addition, EBSD data can be used to investigate the dynamic recrystallization mechanism active during the welding process [6,7].

2. Experimental Procedure

Samples examined for this study were sectioned from 25 mm-thick plate of alloy 2519-T87 aluminum that had been single-pass friction-stir welded. Welding was performed by the Navy Joining Center in Columbus, OH with a tool rotational speed of 175 revolutions/min., and translational speed of 1.5 mm/s. Transverse sections were metallographically prepared and either etched with Keller's reagent or chem-polished with an acetic acid/hydrochloric acid solution at 0 °C. In addition, 3 mm-diameter cylinders from local regions of interest were cored by electro-discharge machining, sliced, and then electropolished with a solution of 30% HNO_3 in methanol at –30 °C and 23 V (67 mA). Local texture measurements by automated EBSD used the TSL OIM system [8] on a LEO 1500 FEG-SEM. Analysis of the microtexture was accomplished using OIM software. Bulk texture measurements were performed on a Scintag X-ray system using Fe Kα radiation and a Huber goniometer. Analysis of bulk texture was completed with the popLA texture package [9].

3.0 Results and Discussion

3.1 Baseline Texture

Bulk texture results from the as-received hot-rolled 2519 aluminum plate reveal the dominant orientation components contain <001> normal to the rolling plane. Figure 1 shows these x-ray texture results in the form of 111 and 100 pole figures recalculated from the orientation distribution function. This texture forms the basis for analysis of subsequent evolution due to FSW-derived thermomechanical processing. Quantitative texture analysis reveals the strongest orientation components, as referenced to the rolling-plane normal sample orientation, to consist of {100}<013>, cube {100}<001>, and Goss {110}<001>.

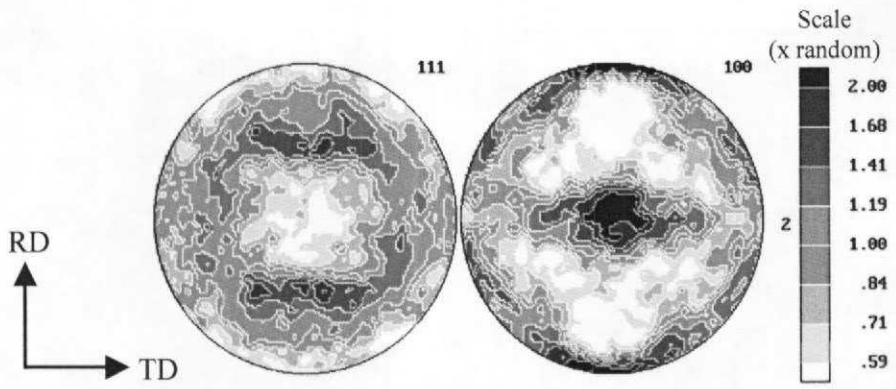

Figure 1: Bulk texture of Al-2519 T87 25 mm plate, showing a <001> near-fiber texture. Recalculated 111 and 100 pole figures, equal-area projection, rolling-plane normal.

However, the overall bulk texture was relatively weak, with a maximum pole figure intensity of approximately 3 times-random.

3.2 EBSD Scans

The texture alteration resulting from material flow into the stir region was investigated through a series of EBSD scans from the base plate, through the HAZ, TMAZ, and into the weld nugget. Two different cross-sections from the Al-2519 FSW were analyzed. Figure 2 shows a schematic of the relative positions of the scanned regions on the first weld cross-section, which concentrated on the advancing side. For this section, the evolution from TMAZ to recrystallized nugget was emphasized. The origin of the reference position (zero) is referred to the TMAZ/nugget interface.

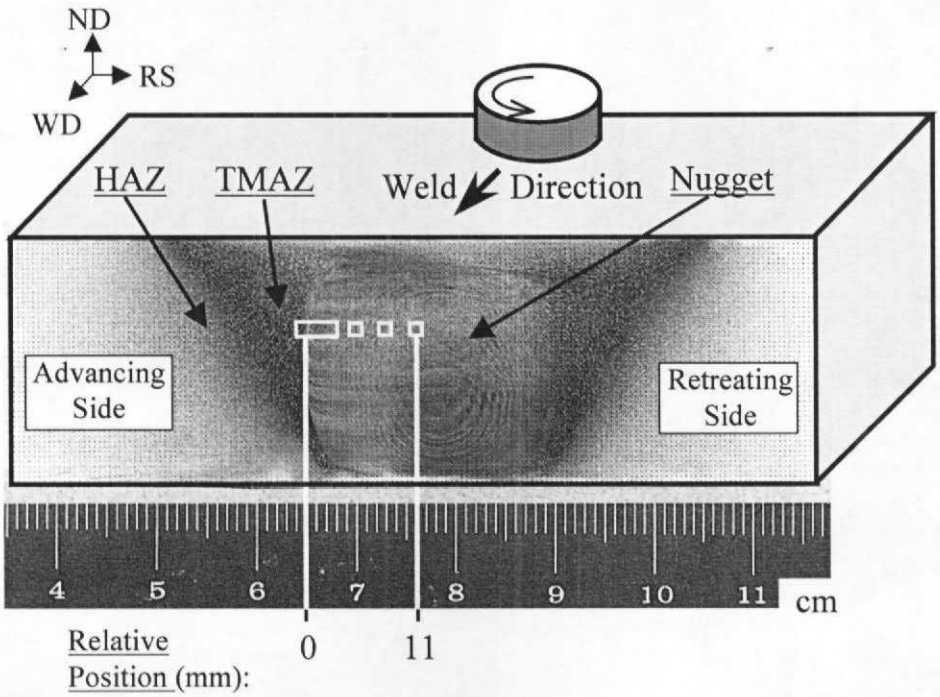

Figure 2. Annotated macrograph from Al-2519 FSW cross-section 1, indicating relative locations of EBSD characterization with respect to weld features. WD = weld direction, RS = retreating side, and ND = normal direction.

Both high-resolution (approximately 0.5 to 1 μm step-size) and low-resolution (5 μm step-size) scans were performed in these regions. Figure 3 shows the EBSD results from a 3 mm-wide low-resolution scan encompassing the TMAZ/nugget interface in the form of a crystal-direction map. Grain boundaries with greater than 15° misorientation are delineated with black lines, and TMAZ material can be identified by elongated grains aligned with their major axis inclined toward the vertical. The grain elongation does not vary appreciably from that of the base plate. However, the inclination increases with proximity to the nugget as base plate material is extruded upward. Details of this flow would vary depending on the vertical (height) position in the plate and the relative influence of the tool shoulder and bottom boundary. The abrupt transition between deformed and recrystallized material is evidence of the steep microstructural gradients present during the FSW process. Texture evolution between the TMAZ and nugget is not obviously evident from relatively coarse interrogations such as that of Fig. 3.

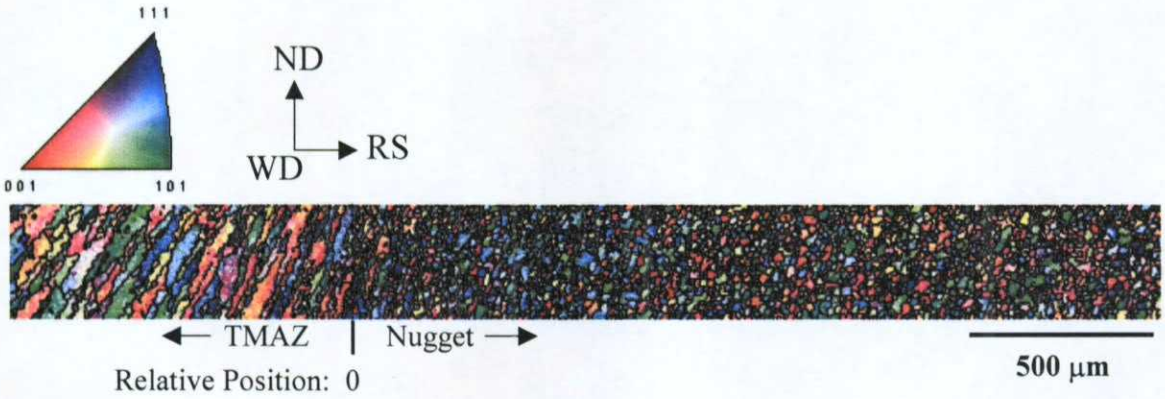

Figure 3: Crystal-direction map with respect to sample weld direction of TMAZ edge at advancing side of friction-stir weld in 2519 Al. Crystal directions are color-keyed to standard projection for cubic crystals.

In order to examine texture gradients in more detail, individual high-resolution EBSD scans were performed at the locations indicated in Fig. 2. Texture results are condensed in Figure 4 in the form of 111 pole figures as a function of transverse position. Simple shear deformation texture development in fcc metals [10] produces two chief components, the 'A' fiber that derives from a rotation of {111} (slip plane) poles into the shear plane, and the 'B' fiber from the alignment of <110> (slip direction) in the shear direction. These components have been previously described in the context of FSW [3,4], and 111 pole figures conveniently highlight the major components. The expected shear plane at the edge locations analyzed here would be aligned perpendicular to the section plane, with its normal in the horizontal direction (tangential to the rotating tool edge). The 'A' component in the 111 pole figures would then be expected to rotate to positions aligned parallel to the vertical axis of the pole figures. This is weakly indicated in the TMAZ regions, but the relationship degrades upon crossing over to the recrystallized nugget. In addition, the rigid rotation of grains within the TMAZ convolutes the effect of shear and that of rigid grain rotation, as will be subsequently addressed. As the weld center is approached the shear plane is expected to rotate towards the transverse section plane. The resultant rotation of 111 poles toward the periphery of the pole figures is weakly observed in Fig. 4.

The more revealing result from the texture gradient is the potential effect of recrystallization on texture. Over distances on the order of 1 mm the texture evolves from that representative of the TMAZ, through a narrow transition zone, into a less developed texture within the nugget that gradually evolves toward the weld center. The nugget texture is characterized by the generation of a near <111> aligned in the horizontal plane and <110> aligned with WD. This is consistent with a 'B' fiber if the shear plane was now aligned with the tool shoulder (original rolling plane). At the vertical position analyzed in cross-section 1 it is conceivable that the shear developed from the tool shoulder may influence texture development at the nugget location. This texture grows somewhat weaker as the weld center is approached.

In order to discriminate between the effects on texture due to changes in shear *versus* those resulting from the recrystallization event, the TMAZ/nugget transition region was analyzed in more detail. Figure 5a shows a crystal-direction map of the transition zone. Recrystallized grains are identified by their equiaxed dimensions, in contrast to the elongated TMAZ grains. The recrystallization mechanism in heavily strained, hot-worked aluminum has been attributed to either continuous dynamic recrystallization (CDRX) or geometric dynamic recrystallization (GDRX) [11-13]. CDRX is established through the generation of high-angle boundaries from low-angle boundaries through dislocation accumulation. GDRX occurs when grains flatten to the order of one-subgrain width at large strains. The original high-angle boundaries become serrated and impinge on themselves, effectively segmenting the original grains. Initial texture, strain path, and strain magnitude all play roles in the details of the recrystallization mechanisms [11]. The EBSD map shows the transition zone is populated by equiaxed grains interspersed with elongated grains. The grain widths are on the order of 25 μm, and some new high-angle boundary segments can be observed within some of the deformed grains.

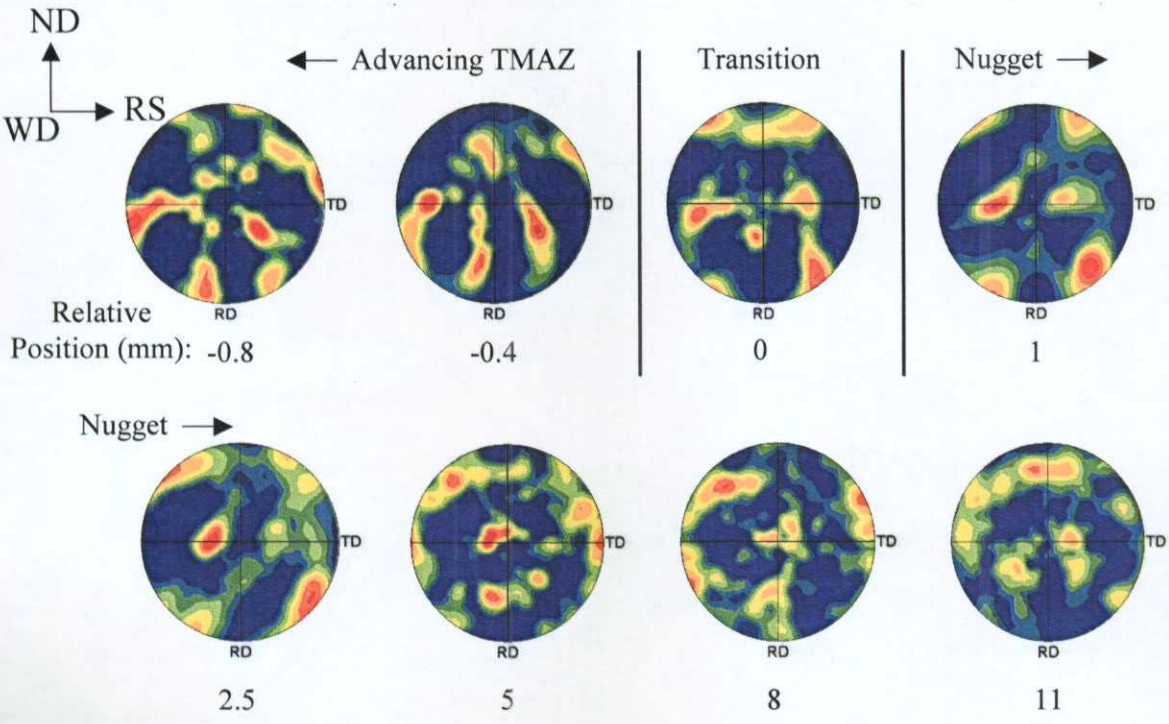

Figure 4. (111) pole figures from EBSD scans of cross-section 1.

From the grain shape aspect-ratio histogram in Fig. 5b the highly aspected and nearly equiaxed tails of the distribution were colored blue and green, respectively. Aspect ratio was defined as the ratio of major-to-minor grain dimensions, such that ideally equiaxed (spherical) grains would have a ratio of unity, and lower values denote greater degrees of elongation. A correlation between elongated grains and dynamic recovery, and equiaxed grains and recrystallization is assumed. As shown in Figure 5c, these grains were also segregated by color on the EBSD map according to aspect ratio. The discrete orientations from the histogram are plotted on a 111 pole figure in Fig. 5d to isolate the orientation change associated with recrystallization. The recrystallized grains roughly exhibit a rotation of 111 about the ND. This evolution is similar to that observed in the transition from TMAZ to nugget for the zoned textures from Fig. 4. Since the spatial location of the grains in Fig. 5 was identical, and therefore the deformation gradient was similar for both sets of orientations, it suggests that the recrystallization process itself produced a measure of discrete texture change. This evolution may inhibit the ability to use textures measured within the nugget to directly deduce the deformation history in a forensic fashion.

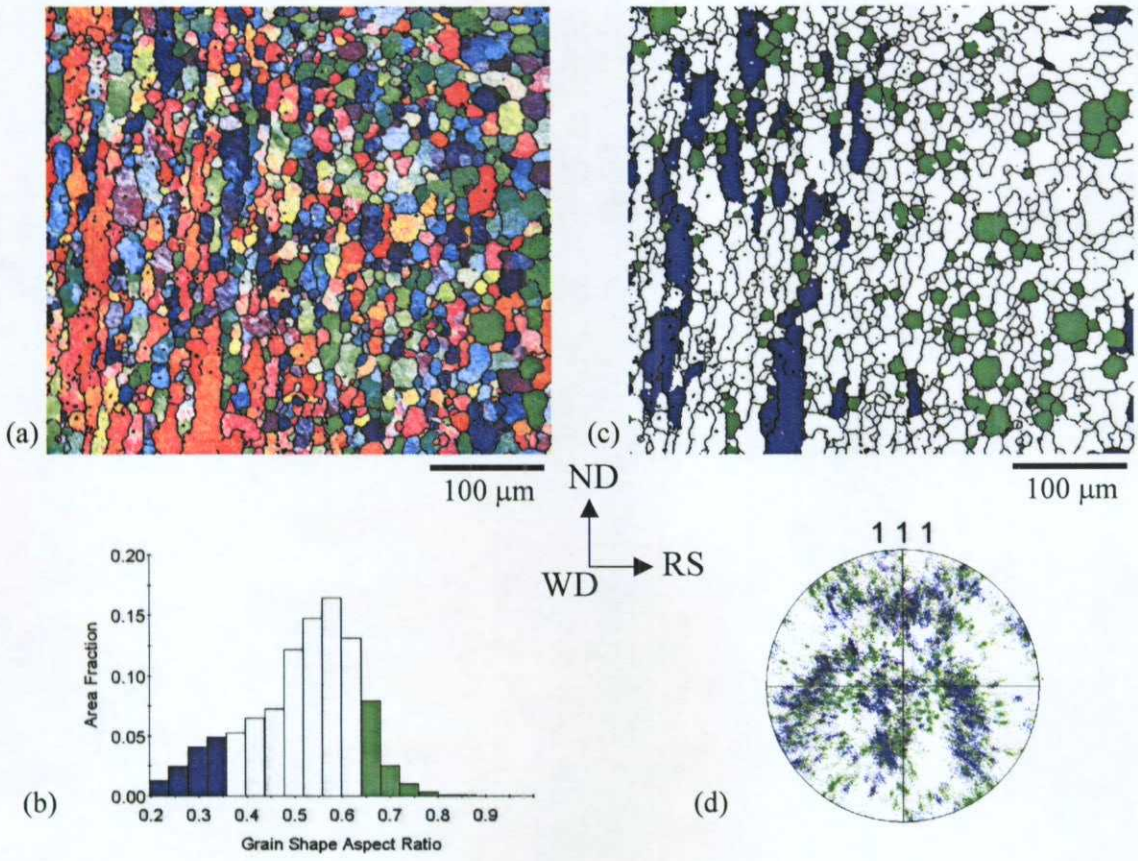

Figure 5. EBSD results from transition region in Al-2519 FSW cross-section 1; a) crystal-direction map with respect to weld direction, color-keyed to standard projection in Fig. 3, b) histogram of grain shape aspect ratios, c) EBSD map with grain shapes segregated by color referenced to histogram, and d) color-referenced (111) discrete pole figure.

EBSD scans were also collected from 3-mm discs representative of various regions from the weld, both on the advancing and retreating sides of the stir zone, as well as through the weld nugget. Figure 6 shows a macrograph of the second weld cross-section with the locations of the representative regions identified. The retreating side of the weld will primarily be discussed for this section. Low-resolution EBSD scans were accomplished *via* stage-control scans in order to define an average texture over the representative area, while high-resolution scans were performed to delineate details of the boundary structure and texture gradients. Pole figures from four regions of the retreating side are shown along with a reference line oriented parallel to the average major axis of elongation for grains in that location. Region 8 (HAZ) displays a grain inclination and texture identical to the base plate, indicating that no deformation was introduced in this region. As the grains are extruded upward the inclination increases progressively toward the weld center, from region 7 at the TMAZ/HAZ boundary to region 5 on the inside of the TMAZ. However, the (111) pole figures exhibit very little evolution due to deformation-induced crystal spin. The majority of the observed differences can instead be attributed to rigid rotation effects, as evidenced by the direct correlation of the pole figure rotation with the changes in grain inclination. This suggests that as material flows upward on the retreating side it either accumulates only modest amounts of strain, or the shear strain is compatible with the initial texture, until very near the nugget region. The texture may be conducive to stabilization of the 'A' component if the shear is perpendicular to the section plane, since the (111) poles would then be contained in the shear plane upon rigid rotation within the TMAZ.

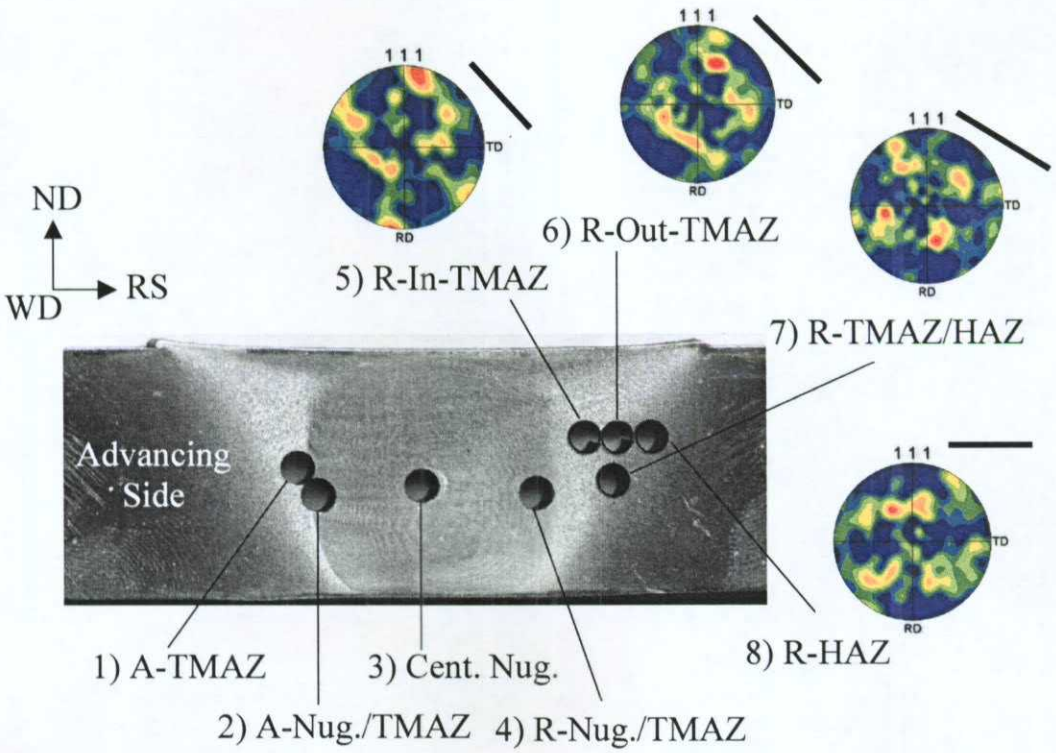

Figure 6. Cross-section 2, showing locations of samples analyzed by EBSD. (111) pole figures and grain aspect direction shown for positions 5-8. 'A' = Advancing side, 'R' = Retreating side.

3.3 Microstructure Statistics as a function of Position in Weld

Several statistics related to microstructural development were compiled for both cross-sections. These included the intragranular orientation spread (IOS), the average grain-to-grain misorientation (for 5° grain misorientation criterion), the fraction of high-angle boundaries (HABs) for all boundaries greater than 5°, and the mean grain size (for 15° grain misorientation criterion). The IOS for each grain is calculated by computing the average misorientation between each orientation and all other orientations within the grain (15° criterion), then taking the mean for all orientations. The overall IOS is then determined as the average spread for all grains in the scan. Figure 7 shows plots of these statistics as a function of relative position for the advancing side in cross-section 1, with relative positions referred to Fig. 2.

The decrease in IOS from the TMAZ to the nugget indicates the effects from dynamic recrystallization (DRX). DRX results in the elimination of low-angle boundaries (LABs) within deformed grains and the generation of HABs between new grains. The process may have initiated at locations farther into the TMAZ; additional scans would be required to verify this. In either case, the recrystallization process as measured by IOS within the scanned regions is completed within a transverse range of approximately 3 mm. This represents a significant alteration in substructure within a very narrow region. The average

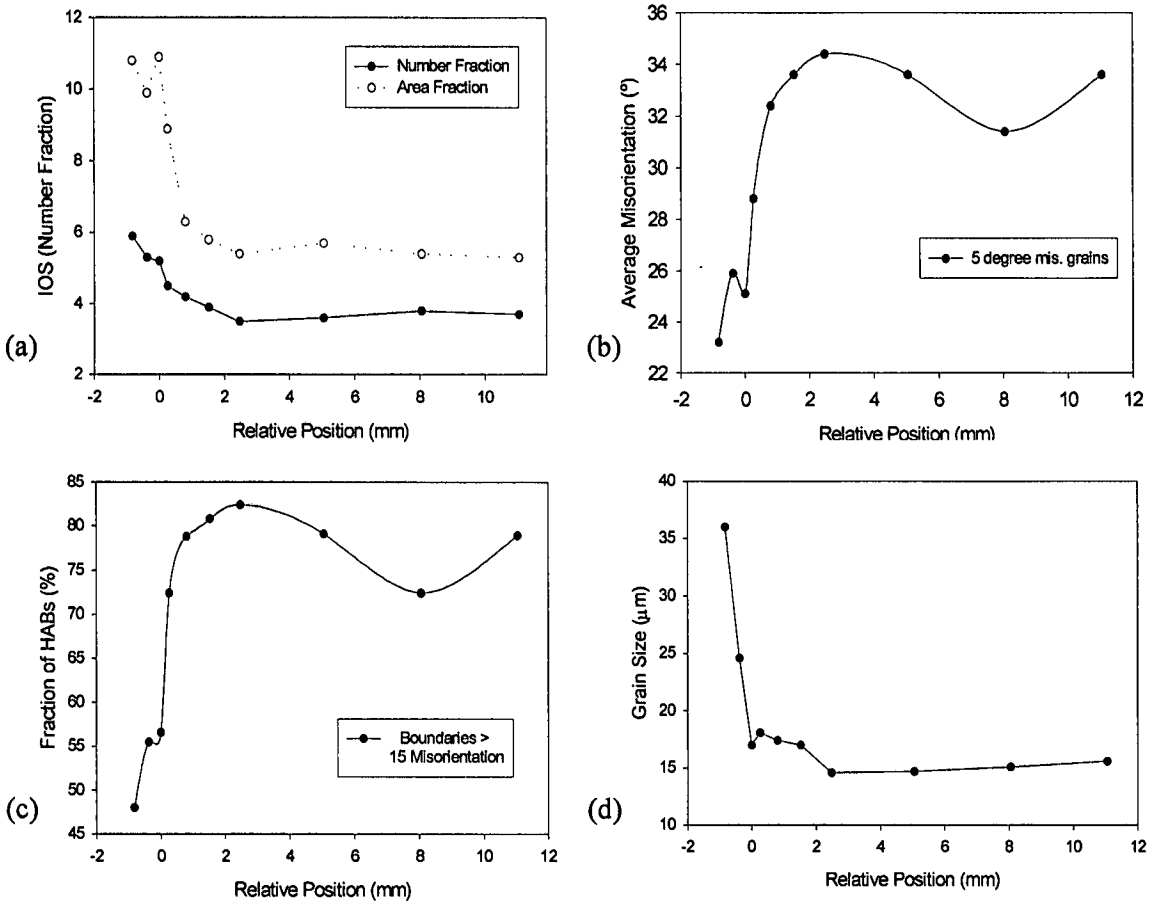

Figure 7: Statistics from EBSD scans of cross-section 1; a) intragranular orientation spread, b) average misorientation, c) fraction of high-angle boundaries, and d) grain size. See text for additional description.

misorientation increases as recrystallization progresses, indicative of the generation of HABs from LABs. A slight decrease in average misorientation occurs as the weld center is approached. This may be due to the spatial variation of stored work in the FSW. At the outer edge of the TMAZ, the thermomechanical work is just sufficient to induce DRX, such that the microstructure is freshly recrystallized. Within other positions in the nugget, the tool rotation may have resulted in additional stored work being accumulated following DRX. At the weld center the average misorientation increases again to a level comparable to nearer the TMAZ edge. The fraction of HABs follows a similar pattern, and reaches a maximum of over 80% at the position corresponding to the greatest average misorientation, once again suggesting the transformation of LABs into HABs. Gourdet and Montheillet [11] correlated the progression of CDRX in aluminum with an evolution of the misorientation distribution from bimodal with a large fraction of LABs at small strains to a flatter distribution with more HABs and an increase in average misorientation of 8° with increased strain ($\varepsilon = 1.5$). The present data agree with the CDRX description of misorientation distribution evolution. As expected, grain refinement occurs in step with the increase in HABs and average misorientation. The greatest effect on grain refinement is accomplished at the far edge of the TMAZ, where HAB generation has just initiated.

In similar fashion the same microstructure statistics were compiled for individual scans from cross-section 2 for locations on both the advancing and retreating sides, and these are plotted in Fig. 8. For the retreating side, sample coverage was sufficient to provide a

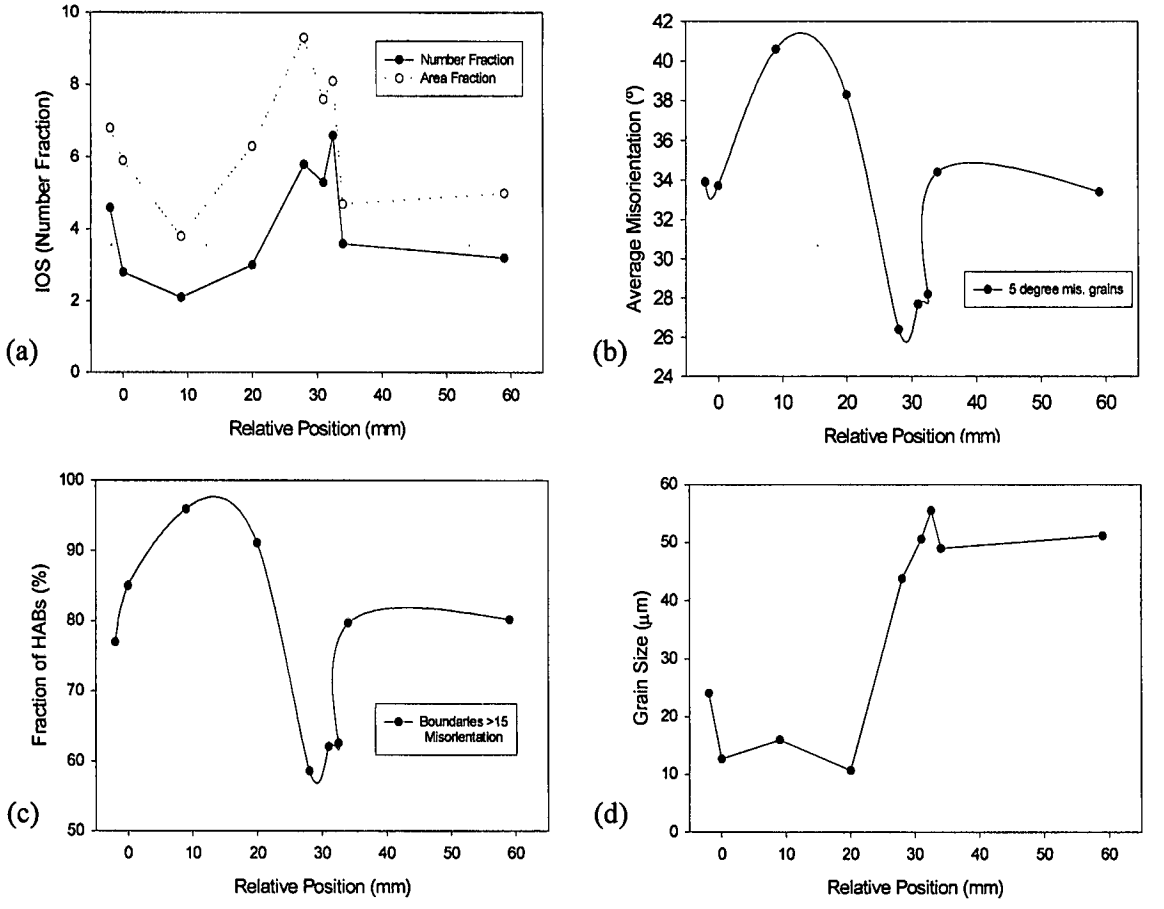

Figure 8: Statistics from EBSD scans of cross-section 2; a) intragranular orientation spread, b) average misorientation, c) fraction of high-angle boundaries, and d) grain size. See text for additional description.

continuous transition from the base plate through the nugget, while the advancing side is represented only at the TMAZ edge, which remains the origin for the relative position scale. The minimum IOS and maximum misorientation and HAB fraction is observed in the center of the nugget, as expected. The maximum IOS is correlated with the retreating side; however, the magnitude is similar to that found for the advancing TMAZ edge in cross-section 1. Therefore, the asymmetry between TMAZ sides in cross-section 2 could be attributable to the sampling of dissimilar relative positions. The minima for misorientation and HAB fraction are correlated with the retreating TMAZ. Symmetry about the nugget for these statistics may be present, but additional sampling from the advancing side would be required to elucidate this. The nugget is represented by greater average misorientation and HAB fraction, and finer grain size, compared to the base plate. This indicates the permanent effect of DRX on the original structure. Furthermore, the effect of the HAZ on structure is observed to be negligible, as these values are nearly identical to those of the base plate. The potency of DRX on grain size refinement is indicated by a decrease from the mid-50 μm range in the base plate to 10-15 μm in the nugget.

For both cross-sections it is evident a significant degree of substructure alteration occurs in the TMAZ. However, the texture was observed to undergo minimal evolution through these regions. Research on aluminum alloys [11-12] has shown a very strong effect of orientation on details of substructure development, and as previously stated, the resultant recrystallization mechanism. Depending on the strain path certain orientations are also very stable with respect to texture evolution and/or resistance to recrystallization. This may explain the texture transition upon recrystallization, as the more stable orientations remain unsegmented by HABs, and may also explain the sluggish deformation texture evolution. Additional investigations are required to determine if this is indeed the case.

4. Conclusions

EBSD measurement and analysis was performed from several locations along a 2519 aluminum FSW. Details concerning the evolution of the microstructure as a function of transverse position were revealed, and these were considered within the context of the deformation produced by the rotating tool. The following features regarding the effect of FSW on microstructural development were determined:

- The advancing-side TMAZ/nugget transition, as defined by grain elongation, occurred over a very narrow (< 1 mm) range.
- The transition region was associated with a texture change that is at least partially attributable to the dynamic recrystallization process. The texture evolution in this region was less a function of position, and therefore deformation gradient, than grain shape aspect ratio.
- Texture evolution from the base plate through the TMAZ may be primarily attributable to rigid rotation of the grains as they are drawn toward the plate surface. However, misorientation distribution evolution suggests substantial substructure development associated with deformation. This may be reconciled if the base plate texture is stable with respect to the simple shear deformation gradient.
- Statistics on the misorientation distribution evolution, along with EBSD maps, suggest that the continuous dynamic recrystallization mechanism is active rather than a geometric DRX. Average misorientations between and within grains progressively increase through the TMAZ, then abruptly decrease into the nugget.

5. Acknowledgments

The material for this study was supplied by the Navy Joining Center/Edison Welding Institute in Columbus, OH. The authors gratefully acknowledge G. Spanos of the Naval Research Laboratory and H. Castner, T. Trapp, and T. Stotler of NJC/EWI for insightful discussions. This work was supported by funding through the Industrial Programs Office of the Office of Naval Research (Steve Linder, Program Manager). One of the authors (JFB) is also supported through the U.S. Department of Energy, under the auspices of the Joint Munitions Program at Los Alamos National Laboratory under Contract W-7405-Eng-36.

6. References

1) H. Jin, S. Saimoto, M. Ball, and P.L. Threadgill, "Characterization of microstructure and texture in friction stir welded joints of 5754 and 5182 aluminum alloy sheets", *Mat. Sci. Tech.*, **17** (2001) 1605-1614.
2) Y. Li, L.E. Murr, and J.C. McClure, "Flow visualization and residual microstructures associated with the friction-stir welding of 2024 aluminum to 6061 aluminum", *Mat. Sci. Eng. A*, **271** (1999) 2213-223.
3) Y.S. Sato, H. Kokawa, K. Ikeda, M. Enomoto, S. Jogan, and T. Hashimoto, "Microtexture in the friction-stir weld of an aluminum alloy", *Met. Mat. Trans. A*, **32** (2001) 941-948.
4) D.P. Field, T.W. Nelson, Y. Hovanski, and K.V. Jata, "Heterogeneity of crystallographic texture in friction stir welds of aluminum", *Met. Mat. Trans. A*, **32** (2001) 2869-2877.
5) B. L. Adams, S. I. Wright, K. Kunze, "Orientation imaging: the emergence of a new microscopy", *Metall. Trans. A*, **24** (1993) 819.
6) K.V. Jata and S.L. Semiatin, "Continuous dynamic recrystallization during friction stir welding of high strength aluminum alloys", *Scripta Mat.*, **43** (2000) 743-749.
7) A.F. Norman, I. Brough, and P.B. Prangnell, "High resolution EBSD Analysis of the grain structure in an AA2024 friction stir weld", *Matls. Sci. Forum*, **331-337** (2000) 1713-1718.
8) TSL/EDAX Orientation Imaging Microscopy manual, Draper, UT 2001.
9) J.S. Kallend, U.F. Kocks, A.D. Rollett, and H.-R. Wenk, "Operational Texture Analysis", *Mat. Sci. Eng. A*, **132** (1991) 1-11.
10) G.R. Canova, U.F. Kocks, and J.J. Jonas, "Theory of torsion texture development", *Acta met.*, **32** (1984) 211-226.
11) S. Gourdet and F. Montheillet, "An experimental study of the recrystallization mechanism during hot deformation of aluminum", *Mat. Sci Eng. A*, **283** (2000), 274-288.
12) M.R. Barnett and F. Montheillet, "The generation of new high-angle boundaries in aluminum during hot torsion", *Acta Mat.*, **50** (2002) 2285-2296.
13) M.E. Kassner, M.M. Myshlyaev, and H.J. McQueen, "Large-strain torsional deformation in aluminum at elevated temperatures", *Mat. Sci. Eng. A*, **108** (1989) 45-61.